# Standard Paleointensity Definitions
# v1.0

February 24, 2014

# Contents

# 1 Preface

Obtaining reliable paleointensity estimates is an important endeavor for understanding the behaviour of the geomagnetic field, but even after almost 70 years of experimentation, it still remains one of the most challenging aspects of modern paleomagnetism. The problems and pitfalls of paleointensity studies are well documented in the literature and great efforts have been made to solve or circumvent many of these issues. One of main tools in achieving this, is a suite of statistics that we can use to quantify and select what we believe to be the most reliable data.

Sadly, it is all too common, even in the modern literature, to find ambiguous descriptions of selection statistics and procedures, or situations where statistics are inconsistently calculated between different studies. Therefore, in an effort to promote consistency in data analysis and reporting, when have compiled the Standard Paleointensity Definitions (SPD), which presents an extensive list of detailed textual and mathematical definitions for paleointensity statistics to aid analysts. SPD not only lists these statistics, but provides numerical and computational advice on how to appropriately and efficient analyze paleointensity data.

SPD is intended to be a useful reference document for the paleomagnetic community and we hope that the community will take up on SPD and contribute to its development. If readers have comments, suggestions, corrections, or criticisms, we warmly invite them to contact us as we would appreciate all input that can help to further improve our ability to consistently select reliable paleointensity data. Maintenance and updating of SPD, however, is our responsibility and we are accountable for any mistakes and omissions (particularly GAP!). The latest and legacy versions of SPD are available at `http://www.paleomag.net/SPD` or `http://earthref.org/PmagPy/SPD`.

If you do use SPD in your work, please make it clear what version was used. For example, by stating "paleointensity statistics were calculated following the Standard Paleointensity Definitions v1.0" or "paleointensity data were analyzed using software X (citing the appropriate reference), which follows the conventions laid out by the Standard Paleointensity Definitions v1.0". We would also be grateful if you cited the publication that introduced the SPD: Paterson, G. A., L. Tauxe, A. J. Biggin, R. Shaar, and L. C. Jonestrask (2014), On improving the selection of Thellier-type paleointensity data, *Geochem. Geophys. Geosyst.*, doi: 10.1002/2013GC005135..

Lastly, throughout our work we have benefited from the ideas and discussions from countless others. All of these have helped to shape SPD in ways both small and large. We want to thank Julie Bowles, Fabio Donadini, Roman Leonhardt, Adrian Muxworthy, Peter Selkin, Hidefumi Tanaka, and Yuhji Yamamoto for their generosity in providing data.

Greig A. Paterson (greig.paterson@mail.iggcas.ac.cn)
Institute of Geology & Geophysics, Chinese Academy of Science, China.

Lisa Tauxe
University of San Diego, USA.

Andrew J. Biggin
University of Liverpool, UK.

Ron Shaar and Lori C. Jonestrask
University of San Diego, USA.

February 24, 2014

# 2 Version history

**Pre-v1.0**
Draft versions during development.

**v1.0** – February 24, 2014
The first finalized version of SPD, published along side Paterson, G. A., L. Tauxe, A. J. Biggin, R. Shaar, and L. C. Jonestrask (2014), On improving the selection of Thellier-type paleointensity data, *Geochem. Geophys. Geosyst.*, doi: 10.1002/2013GC005135..

# 3 Arai plot statistics

## 3.1 A note on data indexing

**Statistic:** $i$ **and** $n_{max}$
The index $i$ is used to denote the $i^{th}$ temperature step of the paleointensity experiment. $i$ is used to index Arai plot data (e.g., $x_i$, or $y_i$) and ranges from $i = 1$ to $n_{max}$, where $n_{max}$ is the total number of steps on the Arai plot.

**Statistic:** *start* **and** *end*
*start* and *end* denote the $i$ indices of the selected steps used for analyzing the paleointensity results. $i = start$ denotes the first selected data point and $i = end$ denotes the last.

**Statistic:** $T_{min}$ **and** $T_{max}$
The minimum and maximum temperatures used for the best-fit linear segment on the Arai plot, where $T_{min} \equiv T_{i=start}$ and $T_{max} \equiv T_{i=end}$.

**Statistic:** $n$
The number of points on an Arai diagram used to estimate the best-fit linear segment and the paleointensity ($n = end - start + 1$).

## 3.2 The paleointensity estimate

**Statistic:** $b$
*Report to 3 d.p.*

The slope of the best-fit line of the selected TRM and NRM points on the Arai plot. Determination of the slope uses the standardized major axis form of least squares linear fitting (*York*, 1966; *Coe et al.*, 1978).

$$b = \text{sign}\left\{\sum_{i=start}^{end}(x_i - \bar{x})(y_i - \bar{y})\right\}\left(\frac{\sum_{i=start}^{end}(y_i - \bar{y})^2}{\sum_{i=start}^{end}(x_i - \bar{x})^2}\right)^{\frac{1}{2}},$$

where $\bar{x}$ and $\bar{y}$ are the mean TRM and NRM values of the data selected for the best-fit, that is,

$$\bar{x} = \frac{\sum_{i=start}^{end} x_i}{n},$$

and

$$\bar{y} = \frac{\sum_{i=start}^{end} y_i}{n}.$$

**Statistic:** $\sigma_b$
*Report to 3 d.p.*

The standard error on the slope is given by:

$$\sigma_b = \left( \frac{2 \sum_{i=start}^{end} (y_i - \bar{y})^2 - 2\,|b| \sum_{i=start}^{end} (x_i - \bar{x})(y_i - \bar{y})}{(n-2) \sum_{i=start}^{end} (x_i - \bar{x})^2} \right)^{\frac{1}{2}}$$

***Useful Note...***
It should be noted that the standard line-fitting routines available in most analysis software (e.g., Excel) do not use the standardized major axis fitting routine, but instead use linear regression (sometimes known as ordinary least-squares), whereby only the y-axis residuals are minimized. Given that accurate estimation of the slope is the objective of paleointensity analysis, standardized major axis, as outlined above, is the most appropriate method (e.g., *Warton et al.*, 2006).

**Statistic:** $B_{Anc}$ **and** $\sigma_B$**, the paleointensity estimate and its error**
*Report to 1 d.p.*

A paleointensity estimate is obtained from $B_{Anc} = |b| \times B_{Lab}$, where $B_{Lab}$ is the strength of the laboratory field. The associated standard error of the estimate is given by $\sigma_B = \sigma_b \times B_{Lab}$.

### 3.3 Arai plot statistics

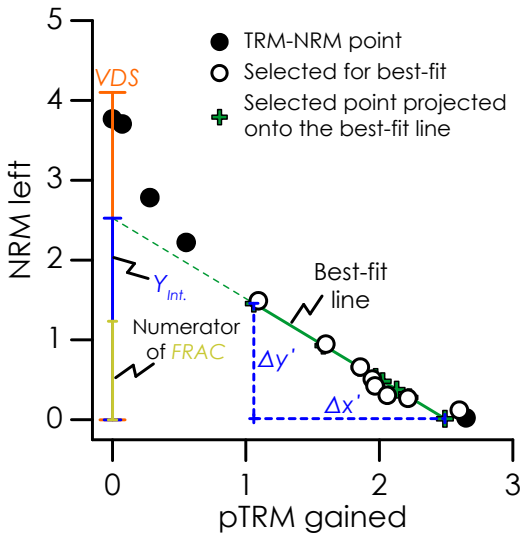


Figure 1: Schematic illustration of an Arai plot and some quantities used in the calculation of paleointensity statistics.

**Statistic:** $Y_{Int.}$
The y-axis (NRM) intercept of the best-fit line on the Arai plot.

$$Y_{Int.} = \bar{y} - b\bar{x}$$

**Statistic:** $X_{Int.}$
The x-axis (TRM) intercept of the best-fit line on the Arai plot.

$$X_{Int.} = \frac{-Y_{Int.}}{b}$$

**Statistic: Vector difference sum,** $VDS$
The vector difference sum of the entire NRM vector (**NRM**).

$$VDS = |\mathbf{NRM}_{n_{max}}| + \sum_{i=1}^{n_{max}-1} |\mathbf{NRM}_{i+1} - \mathbf{NRM}_i|,$$

where $|\mathbf{NRM}_i|$ denotes the length of the NRM vector at the $i^{th}$ step.

**Statistic:** $x'$ **and** $y'$
$x'$ and $y'$ the $x$ and $y$ points on the Arai plot projected on to the best-fit line. These are used to calculate the NRM fraction and the length of the best-fit line among other parameters. There are multiple ways of calculating $x'$ and $y'$, below is one example.

$$x'_i = \frac{1}{2}\left(x_i + \frac{y_i - Y_{Int.}}{b}\right)$$

$$y'_i = \frac{1}{2}\left(y_i + bx + Y_{Int}\right)$$

**Statistic:** $\Delta x'$ **and** $\Delta y'$
$\Delta x'$ and $\Delta y'$ are TRM and NRM lengths of the best-fit line on the Arai plot, respectively (Figure 1).

$$\Delta x' = \left|[\max\{x'_i\} - \min\{x'_i\}]_{i=start,\ldots,end}\right|$$
$$\Delta y' = \left|[\max\{y'_i\} - \min\{y'_i\}]_{i=start,\ldots,end}\right|$$

**Statistic:** $f$
*Report to 3 d.p.*

NRM fraction used for the best-fit on an Arai diagram (*Coe et al.*, 1978).

$$f = \frac{\Delta y'}{|Y_{Int.}|}$$

**Statistic:** $f_{VDS}$
*Report to 3 d.p.*

NRM fraction used for the best-fit on an Arai diagram calculated as a vector difference sum (*Tauxe and Staudigel*, 2004).

$$f_{VDS} = \frac{\Delta y'}{VDS}$$

**Statistic:** *FRAC*
*Report to 3 d.p.*

NRM fraction used for the best-fit on an Arai diagram determined entirely by vector difference sum calculation (*Shaar and Tauxe*, 2013).

$$FRAC = \frac{\sum_{i=start}^{end-1} |\mathbf{NRM}_{i+1} - \mathbf{NRM}_i|}{VDS}$$

**Statistic:** $\beta$
*Report to 3 d.p.*

$\beta$ is a measure of the relative data scatter around the best-fit line and is the ratio of the standard error of the slope to the absolute value of the slope (*Coe et al.*, 1978).

$$\beta = \frac{\sigma_b}{|b|}$$

**Statistic:** $g$
*Report to 3 d.p.*

The gap factor ($g$) is a measure of the average NRM lost between successive temperature steps of the segment chosen for the best-fit line on the Arai plot. The gap reflects the average spacing of the selected Arai plot points along the best-fit line.

$$g = 1 - \frac{\sum_{i=start}^{end-1} \left(y'_{i+1} - y'_i\right)^2}{\Delta y'^2}.$$

The upper limit of $g$ is dependent on $n$ and occurs when the points on the Arai plot are evenly spaced.

$$g_{lim} = \frac{n-2}{n-1}.$$

**Statistic:** *GAP-MAX*
*Report to 3 d.p.*

The gap factor defined above is measure of the average Arai plot point spacing and may not represent extremes of spacing. To account for this *Shaar and Tauxe* (2013) proposed *GAP-MAX*, which is the maximum gap between two points determined by vector arithmetic.

$$GAP\text{-}MAX = \frac{\max\left\{|\mathbf{NRM}_{i+1} - \mathbf{NRM}_i|\right\}_{i=start,\ldots,end-1}}{\sum_{i=start}^{end-1} |\mathbf{NRM}_{i+1} - \mathbf{NRM}_i|}$$

**Statistic:** $q$
*Report to 1 d.p.*

The quality factor ($q$) is a measure of the overall quality of the paleointensity estimate and combines the relative scatter of the best-fit line, the NRM fraction and the gap factor (*Coe et al.*, 1978).

$$q = \frac{|b|\, fg}{\sigma_b} = \frac{fg}{\beta}$$

**Statistic:** $w$
*Report to 1 d.p.*

Weighting factor of *Prévot et al.* (1985).

$$w = \frac{fg}{s},$$

where $s^2$ is given by:

$$s^2 = 2 + \frac{2\sum_{i=start}^{end}(x_i - \bar{x})(y_i - \bar{y})}{\left(\sum_{i=start}^{end}(x_i - \bar{x})^{\frac{1}{2}} \sum_{i=start}^{end}(y_i - \bar{y})^2\right)^2}.$$

It can be noted, however, that $w$ can be more readily calculated as:

$$w = \frac{q}{\sqrt{n-2}}.$$

**Statistic:** $\left|\vec{k}\right|$
*Report to 3 d.p.*

The curvature of the Arai plot as determined by the best-fit circle to all of the data (*Paterson*, 2011). To determine the Arai curvature, a best-fit circle of the form $(x-a)^2+(y-b)^2 = r^2$ is fitted to all of the data using a least-squares approach. For the fitting process, each axis is normalized by the maximum value of the data on that axis such that $0 \leq \text{TRM} \leq 1$, and $0 \leq \text{NRM} \leq 1$, which ensures a consistent comparison between data measured with different $B_{Lab}$. $\left|\vec{k}\right|$ is defined as the reciprocal of the radius ($r$) of the best-fit circle:

$$\left|\vec{k}\right| = \frac{1}{r}.$$

Curvature can be given a sense of direction by considering the position of the circle center $(a, b)$ with respect to the centroid of all of the data $(C_x, C_y)$.

$$\vec{k} = \begin{cases} \frac{1}{r} & \text{if } (C_x < a) \textit{ and } (C_y < b) \\ -\frac{1}{r} & \text{if } (a < C_x) \textit{ and } (b < C_y) \\ 0 & \text{if } (a = C_x) \textit{ and } (b = C_y) \end{cases}.$$

***Numerical Tip...***
Standard non-linear line fitting routines can be used for the calculation of the best-fit circle to the Arai plot data, however, the convergence of these algorithms can be poor and they are often numerically inaccurate when the data form a small arc of a much larger circle. This latter point is particularly important for near linear Arai plots as the data represent an increasingly smaller arc of the circle as the linearity increases. *Chernov and Lesort* (2005) developed an algorithm for fitting circles to data that is less affected by both of these issues and should be the preferred method of circle fitting (*Paterson*, 2011). Code for this algorithm in `C++` and `MATLAB` are available from `http://www.paleomag.net/SPD/downloads.html`.

**Statistic:** *SSE*
*Report to 3 d.p.*

The quality of the best-fit circle used to determine $\left|\vec{k}\right|$ (*Paterson*, 2011).

$$SSE = \sum_{i=1}^{n_{max}} \left( \sqrt{(x_i - a)^2 + (y_i - b)^2} - r \right)^2$$

Where $x_i$ and $y_i$ denote the normalized TRM and NRM, respectively.

**Statistic:** *SCAT*
*SCAT* is a parameter proposed by *Shaar and Tauxe* (2013) in an effort to reduce the number of parameters used to quantify a paleointensity estimate. *SCAT* is a Boolean operator, which uses the error on the best-fit Arai plot slope to indicate whether the data over the selected range are too scattered or not. This parameter provides a test for the scatter of the points on the Arai plot, pTRM checks, and pTRM tail checks. A schematic illustration of *SCAT* and some examples are shown in Figure 2.

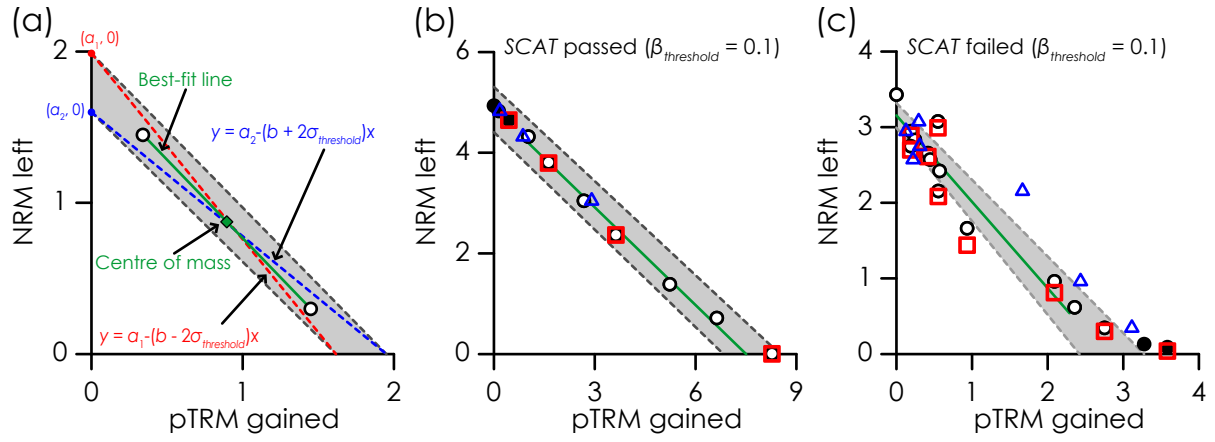


Figure 2: (a) Schematic illustration of the calculation of the *SCAT* box. Examples of data that (b) pass and (c) fail *SCAT*. In all examples the gray shaded area is the *SCAT* box. In parts (b) and (c) open (closed) circles denote the selected (unselected) points. The triangles and squares represent pTRM checks and pTRM tail checks, respectively.

First, from the chosen the best-fit segment on the Arai plot, the slope ($b$), the standard error of the slope ($\sigma_b$), and $\beta \left(= \frac{\sigma_b}{|b|}\right)$ are obtained. For a given sample, the threshold value for $\beta$ that is used to select data ($\beta_{threshold}$) is used to determine an equivalent threshold for $\sigma_b$ ($\sigma_{threshold} = |b|\,\beta_{threshold}$).

$b$ and $\sigma_{threshold}$ are then used to determine two lines that pass through the center of mass of the selected Arai plot segment ($\bar{x}$ and $\bar{y}$), one with a slope of $b + 2\sigma_{threshold}$, the other with a slope of $b - 2\sigma_{threshold}$ (Figure 2a). The so called *SCAT* box, is the box that is defined by the four intercepts that the above two lines make with the x- and y-axes (Figure 2a).

If all the data points associated with the chosen Arai plot segment, which includes both pTRM and tail checks, fall within the *SCAT* box then *SCAT* is *TRUE*. If one or more points fall outside the *SCAT* box then *SCAT* is *FALSE*. Samples are accepted only if *SCAT* is *TRUE*. pTRM checks and pTRM tail checks are included in the calculation of *SCAT* if the temperature of the check

falls within temperature range of the selected Arai plot segment and the peak temperature before the check was performed is less than or equal to maximum temperature of the selected Arai plot segment. For example, if the temperature range of the selected Arai plot segment was 100–500°C, a pTRM check to 200°C performed after the 400°C step would be included in the calculation of $SCAT$. However, a pTRM check to 200°C performed after the 540°C would be *not* included in the calculation of $SCAT$. Examples of samples pass and fail $SCAT$ are shown in Figure 2b and c, respectively.

**Statistic:** $R^2_{corr}$
*Report to 3 d.p.*

The correlation coefficient to estimate the strength of the linear relationship between the NRM and TRM over the best-fit Arai plot segment (the square of the Pearson correlation).

$$R^2_{corr} = \frac{\left(\sum_{i=start}^{end}(x_i - \bar{x})(y_i - \bar{y})\right)^2}{\sum_{i=start}^{end}(x_i - \bar{x})^2 \sum_{i=start}^{end}(y_i - \bar{y})^2}$$

**Statistic:** $R^2_{det}$
*Report to 3 d.p.*

Coefficient of determination to estimate variance accounted for by the linear model fit.

$$R^2_{det} = 1 - \frac{\sum_{i=start}^{end}(y_i - y'_i)^2}{\sum_{i=start}^{end}(y_i - \bar{y})^2}$$

***Useful Note...***
It should be noted that this is similar to, but strictly not the same as the square of the Pearson correlation coefficient ($R^2_{corr}$). For least squares fitting that minimizes the y residuals only, $R^2_{corr}$ is the same as the coefficient of determination for the model fit. Since Arai plot analysis uses the standardized major axis least-squares variant, this is not the case. For most practical purposes, however, the difference is small, particularly when the chosen Arai plot segment is highly linear with low noise.

**Statistic:** $Z$ **and** $Z^*$
*Report to 1 d.p.*

$Z$ is an Arai plot zigzag parameter defined by *Yu and Tauxe* (2005).

$$Z = \sum_{i=start}^{end} \frac{x_i \left|\tilde{b}_i - |b|\right|}{|X_{Int.}|},$$

where $\tilde{b}_i$ is the instantaneous slope on the Arai plot determined from the ratio of the NRM lost to the TRM gained at the $i^{th}$ step:

$$\tilde{b}_i = \frac{NRM_{total} - NRM_i}{TRM_i} = \frac{Y_{Int.} - y_i}{x_i}.$$

Since no TRM is gained during the first step $\tilde{b}_1 = 0$. $\tilde{b}_i - |b|$ is a measure of the scatter around the best-fit slope on the Arai plot.

*Yu* (2012) proposed a modified version, $Z^*$.

$$Z^* = \frac{1}{n-1} \sum_{i=start}^{end} 100 \times \frac{x_i \left| \tilde{b}_i - |b| \right|}{|Y_{Int.}|}.$$

**Statistic:** $IZZI\_MD$
*Report to 3 d.p.*

$IZZI\_MD$ is a parameter to quantify the zigzagging on an Arai plot (*Shaar et al.*, 2011), which is most pronounced for multidomain grains measured with the IZZI protocol (e.g., *Yu et al.*, 2004).

$IZZI\_MD$ is a measure of the area mapped out on the Arai plot and is determined using all the points on an Arai plot with the exception of the first step, where no TRM is imparted. The calculation is performed after the points have been normalized by the initial NRM, such that

$$x_{(n)i} = \frac{x_i}{y_1} \quad \text{and} \quad y_{(n)i} = \frac{y_i}{y_1}.$$

If we consider the three consecutive Arai plot points illustrated in Figure 3a. The lengths of each side of the triangle formed by these points are given by:

$$L_1 = \sqrt{\left(x_{(n)i} - x_{(n)i+1}\right)^2 + \left(y_{(n)i} - y_{(n)i+1)}\right)^2};$$

$$L_2 = \sqrt{\left(x_{(n)i+1} - x_{(n)i+2}\right)^2 + \left(y_{(n)i+1} - y_{(n)i+2}\right)^2};$$

and

$$L_3 = \sqrt{\left(x_{(n)i+2} - x_{(n)i}\right)^2 + \left(y_{(n)i+2} - y_{(n)i}\right)^2}.$$

Following the cosine rule, the angle $\phi$ is

$$\phi = \arccos\left(\frac{L_2^2 + L_3^2 - L_1^2}{2L_2L_3}\right)$$

The height of the triangle can be expressed as

$$H = L_3 \sin(\phi),$$

and hence the area of the triangle is given by

$$A_i = \frac{L_2 L_3 \sin(\phi)}{2}.$$

Each $A_i$ is given a sign ($\pm$) based on whether or not the ZI steps lie above the IZ steps, or *vice versa*. For ZI above IZ, $A_i$ is positive, for IZ above ZI, $A_i$ is negative. For the example in Figure 3, ZI is above IZ and the area is given a positive sign.

To determine the sign, we must determine the relative position of the mid-point of the three consecutive points. First, we calculate the best-fit line through the first and last points and obtain the intercept of the line ($a_1$; Figure 3b). Using the slope of this best-fit line we determine the intercept of the line ($a_2$) when the line passes through the mid-point. If $a_1$ is less than $a_2$ the mid-point lies above the end points, but if $a_2$ is less than $a_1$ the mid-point lies below the end points. In the case where $a_1 = a_2$ all three points lie on a perfect straight line and both the area and the sign are identically zero. The pseudo-code for this is as follows, where $S_i$ denotes the sign of the $i^{th}$ area.

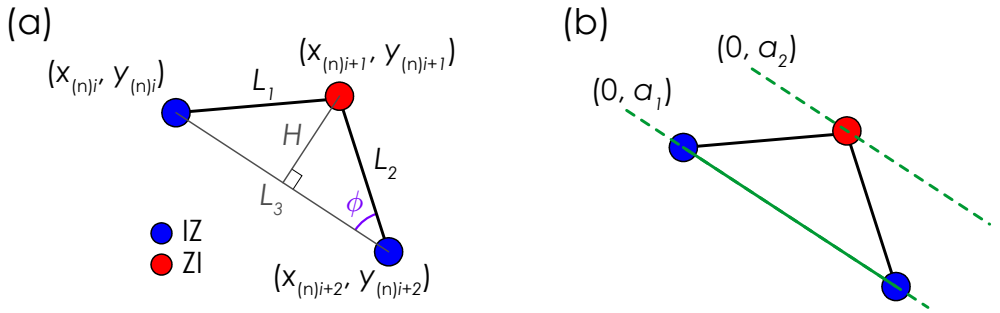


Figure 3: Illustration of the calculation of $IZZI\_MD$. (a) The calculation of the area bounded by three consecutive Arai plot points. (b) The determination of the relative position of the mid-point.

**for** $i = 2 \rightarrow i = n_{max} - 2$ **do**
  **if** $a_1 = a_2$ **then**
    $S_i = 0$
  **else**
    **if** Mid-point is a ZI **then**
      **if** $a_1 < a_2$ **then**
        $S_i = 1$ ←{Figure 3b falls here}
      **else**
        $S_i = -1$
      **end if**
    **else if** Mid-point is a IZ **then**
      **if** $a_1 < a_2$ **then**
        $S_i = -1$
      **else**
        $S_i = 1$
      **end if**
    **end if**
  **end if**
**end for**

$IZZI\_MD$ is the sum of the signed areas, normalized by length of the line connecting all of the ZI steps.

$$IZZI\_MD = \sum_{i=2}^{n_{max}-2} \frac{S_i A_i}{L_{ZI}}.$$

where $L_{ZI}$ is given by:

$$L_{ZI} = \sum_{i \in \ ZI \ points} \sqrt{\left(x_{(n)i+2} - x_{(n)i}\right)^2 + \left(y_{(n)i+2} - y_{(n)i}\right)^2}\ .$$

**N.B.** The $i+2$ increment assumes alternating ZI and IZ step, whereby if $i$ is a ZI step, $i+1$ is an IZ step, and $i+2$ is a ZI step.

***Numerical Tip***...
Calculating the area bounded by a series of points is a common geometric problem. As a consequence most programming languages have functions to perform the calculation either as inbuilt features or as freely available routines. For example, `MATLAB` has the inbuilt function `A=polyarea(p)` to return the area, `A`, bounded by the points given by the two-dimensional matrix `p`:

$$\mathbf{p} = \begin{pmatrix} x_i & y_i \\ x_{i+1} & y_{i+1} \\ x_{i+2} & y_{i+2} \end{pmatrix}$$

# 4 Directional statistics

**Statistic:** *Dec* **and** *Inc*
*Report to 1 d.p.*

The declination (*Dec*) and the inclination (*Inc*) of NRM direction of the paleointensity data over the same range of points used for the paleointensity estimates. *Dec* and *Inc* are calculated using the principal component analysis (PCA) method of *Kirschvink* (1980) and may be obtained from either a free-floating or anchored fit.

The method of applying PCA to paleomagnetic data is as follows. Let $X_{1,i}$, $X_{2,i}$, and $X_{3,i}$ denote the $x$, $y$, and $z$ Cartesian coordinates of the NRM vector of the selected points ($i = start \ldots end$). The center of mass of the data is given by the ordinates $\bar{X}_1$, $\bar{X}_2$, and $\bar{X}_3$.

$$\bar{X}_1 = \frac{\sum_{i=start}^{end} X_{1,i}}{n}; \quad \bar{X}_2 = \frac{\sum_{i=start}^{end} X_{2,i}}{n}; \quad \bar{X}_3 = \frac{\sum_{i=start}^{end} X_{3,i}}{n}$$

The coordinates of the NRM vector are then transformed to be centered about $\bar{X}_1$, $\bar{X}_2$, and $\bar{X}_3$.

$$X'_{1,i} = X_{1,i} - \bar{X}_1; \quad X'_{2,i} = X_{2,i} - \bar{X}_2; \quad X'_{3,i} = X_{3,i} - \bar{X}_3,$$

where $X'_{1,i}$, $X'_{2,i}$, and $X'_{3,i}$ are the transformed coordinates. A fit anchored to the origin of the component diagram can be obtained by setting [$\bar{X}_1$, $\bar{X}_2$, $\bar{X}_3$] to [0, 0, 0].

The orientation tensor, $\mathbf{T}$, of the transformed NRM data is defined as:

$$\mathbf{T} = \begin{pmatrix} \sum X'_{1,i}X'_{1,i} & \sum X'_{1,i}X'_{2,i} & \sum X'_{1,i}X'_{3,i} \\ \sum X'_{1,i}X'_{2,i} & \sum X'_{2,i}X'_{2,i} & \sum X'_{2,i}X'_{3,i} \\ \sum X'_{1,i}X'_{3,i} & \sum X'_{2,i}X'_{3,i} & \sum X'_{3,i}X'_{3,i} \end{pmatrix}.$$

This orientation tensor is usually constructed within sample or geographic coordinates and consists of six independent elements. Typically, none of these elements zero. When the non-diagonal elements of $\mathbf{T}$ are non-zero the vector components described by this coordinate system are not independent, they are correlated. There exists, however, a coordinate system in which the orientation tensor can be expressed in terms of three independent orthogonal components. The axes of this coordinates system are known as the eigenvectors of the matrix and can be expressed in linear algebra form as:

$$\mathbf{TV} = \tau\mathbf{V},$$

where $\mathbf{V}$ is a matrix that contains the three eigenvectors (also know as principal axes) and $\tau$ is a diagonal matrix that contains the three eigenvalues. When ranked by $\tau$, such that $\tau_3 < \tau_2 < \tau_1$, the principal axis (i.e., $\mathbf{V}_1 = [V_{1,x}, V_{1,y}, V_{1,z}]$) corresponds to axis of the characteristic paleomagnetic direction.

***Numerical Tip***...
PCA is a widely used technique and numerous programming languages have inbuilt PCA functions. In `MATLAB`, for example, the command `[V, tau]=eig(T)` returns $\mathbf{V}$ and $\tau$. The equivalent in `Python` is `tau,V=numpy.linalg.eig(T)`.

It should be noted, however, that paleomagnetic direction may be either parallel or anti-parallel to $\mathbf{V}_1$ and the sense of direction must be established. To do this, we define a reference vector ($\mathbf{R}$) defined as the difference between the first and last NRM vector measurements:

$$\mathbf{R} = \mathbf{X}'_{i=start} - \mathbf{X}'_{i=end} = \left[X'_{1,start} - X'_{1,end}, X'_{2,start} - X'_{2,end}, X'_{3,start} - X'_{3,end}\right].$$

The vector dot product of $\mathbf{V}_1$ and $\mathbf{R}$ is then determined.

$$dot = \mathbf{V}_1 \cdot \mathbf{R} = V_{1,x} \times R_x + V_{1,y} \times R_y + V_{1,z} \times R_z$$

The range of *dot* is then truncated to exist only over [-1, 1].

**if** $dot < -1$ **then**
  $dot = -1$
**else if** $dot > 1$ **then**
  $dot = 1$
**end if**

The principal paleomagnetic direction ($\mathbf{PD} = [PD_x, PD_y, PD_z]$ can be given a sense of direction along $\mathbf{V}_1$ as follows.

**if** $\arccos(dot) > \frac{\pi}{2}$
**then**
  $\mathbf{PD} = -\mathbf{V}_1$
**else**
  $\mathbf{PD} = \mathbf{V}_1$
**end if**

The declination ($Dec$) and inclination ($Inc$) of principal paleomagnetic direction can be calculated.

**if** $PD_x < 0$ **then**
  $Dec = \arctan\left(\frac{PD_y}{PD_x}\right) + 180°$
**else if** $PD_x > 0$ **and** $PD_y \leq 0$ **then**
  $Dec = \arctan\left(\frac{PD_y}{PD_x}\right) + 360°$
**else**
  $Dec = \arctan\left(\frac{PD_y}{PD_x}\right)$
**end if**

$$Inc = \arctan\left(\frac{PD_z}{\sqrt{PD_x^2 + PD_y^2}}\right)$$

***Useful Note...***
The choice of free-floating or anchored fit should be stated by using subscripts on $Dec$ and $Inc$. That is, $Dec_{Free}$ and $Inc_{Free}$ for a free-floating fit and $Dec_{Anc.}$ and $Inc_{Anc.}$ for an anchored fit.

**Statistic:** $MAD_{Anc.}$ **and** $MAD_{Free}$
*Report to 1 d.p.*

$MAD_{Anc.}$ and $MAD_{Free}$ are Maximum Angular Deviation (MAD) of the anchored and free-floating, respectively, directional fits to the paleomagnetic vector on a vector component diagram (*Kirschvink*, 1980). Determined from the paleointensity demagnetization steps.

$MAD$ is calculated as:

$$MAD = \arctan\left(\sqrt{\frac{\tau_2 + \tau_3}{\tau_1}}\right),$$

where $\tau_3 < \tau_2 < \tau_1$ are the eigenvalues of the PCA matrix.

**Statistic:** $\alpha$
*Report to 1 d.p.*

Angular difference between the anchored and free-floating best-fit directions on a vector component diagram.

***Numerical Tip...***
Most directional parameters are related to the angle between two vectors. The angle between two vectors (denoted **a** and **b**) can be calculated by a simple rearrangement of the formulation for the dot product:

$$\theta = \arccos\left(\frac{\mathbf{a}\cdot\mathbf{b}}{|\mathbf{a}|\,|\mathbf{b}|}\right).$$

This approach, however, can be prone to numerical inaccuracies when $\theta$ is close to zero or $\pi$. For most practical purposes this should not be an issue, but the following alternative formulation can be used to avoid these inaccuracies:

$$\theta = \arctan\left(\frac{|\mathbf{a}\times\mathbf{b}|}{\mathbf{a}\cdot\mathbf{b}}\right),$$

where $\times$ denotes the vector cross product. The `atan2` function in most programing languages can be used to determine the appropriate quadrant. N.B. The above fraction is equivalent to $\frac{y}{x}$ in the terminology of most `atan2` functions.

**Statistic:** $\alpha'$
*Report to 1 d.p.*

Angular difference between the anchored best-fit direction from the paleointensity experiment and an independent measure of the paleomagnetic direction (*Kissel and Laj*, 2004). The independent direction can be derived from a separate demagnetization experiment or from a known reference direction.

**Statistic:** $\theta$
*Report to 1 d.p.*

The angle between the applied field direction and the ChRM direction of the NRM as determined from the free-floating PCA fit to the selected demagnetization steps of the paleointensity experiment.

**Statistic:** *DANG*
*Report to 1 d.p.*

The Deviation ANGle: the angle between the free-floating best-fit direction and the direction between data center of mass $[\bar{X}_1, \bar{X}_2, \bar{X}_3]$ and the origin of the vector component diagram (*Tanaka and Kobayashi*, 2003; *Tauxe and Staudigel*, 2004).

**Statistic:** $NRM_{dev}$
*Report to 1 d.p.*

The intensity deviation of the free-floating principal component from the origin of the vector component diagram, normalized by the total NRM intensity ($Y_{Int.}$; *Tanaka and Kobayashi*, 2003).

$$NRM_{dev} = \frac{\sin(DANG)\sqrt{\bar{X}_1{}^2 + \bar{X}_2{}^2 + \bar{X}_3{}^2}}{|Y_{Int.}|} \times 100$$

**Statistic:** $\gamma$
*Report to 1 d.p.*

The angle between the pTRM acquired at the last step used for the best-fit segment (i.e., $\mathbf{TRM}_{i=end}$) and the applied field direction ($\mathbf{B}_{Lab}$). $\gamma$ can be used as a quick check to assess if a sample is strongly influenced by anisotropic TRM. See Section 8 for further information of measuring and quantifying anisotropy of TRM.

**Statistic:** $CRM(\%)$
*Report to 1 d.p.*

To detect the potential acquisition of chemical remanent magnetization (CRM), *Coe et al.* (1984) proposed $CRM(\%)$ to measure the deflection the NRM vector towards the direction of $B_{Lab}$ as would be expected during the formation of CRM. A schematic illustration of the quantities involved in the calculation of $CRM(\%)$ are shown in Figure 4. To determine $CRM(\%)$ the characteristic remanent magnetization (ChRM) direction needs to be known. This must be determined from an independent demagnetization experiment.

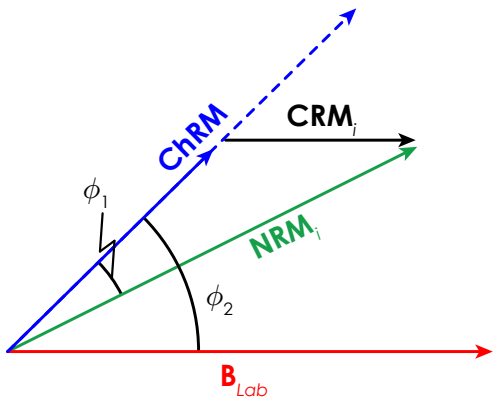


Figure 4: Illustration of an NRM vector ($\mathbf{NRM}_i$) being deflected from the expected ChRM direction toward the applied field direction ($\mathbf{B}_{Lab}$) by the acquisition of CRM during laboratory heating.

First, the magnitude of the CRM vector is determined:

$$CRM_i = \|\mathbf{NRM}_i\| \frac{\sin(\phi_1)}{\sin(\phi_2)} = y_i \frac{\sin(\phi_1)}{\sin(\phi_2)},$$

where $\|\mathbf{NRM}_i\|$ denotes the length of the $\mathbf{NRM}_i$ vector, which is equivalent to $y_i$. $CRM(\%)$ is the maximum value of $CRM_i$ over the selected best-fit Arai segment, normalized by the length of the TRM portion of best-fit Arai line:

$$CRM(\%) = \frac{\max\{CRM_i\}_{i=start,\ldots,end}}{\Delta x'} \times 100.$$

***Useful Note...***
In the original work by Coe $CRM(\%)$ was originally called "$R$". We have renamed this statistic to avoid confusion with the "$R$"'s related to Arai plot linearity and line-fitting ($R^2_{corr}$ and $R^2_{det}$) and the length of the resultant vector when undertaking a Fisher analysis of paleomagnetic directions. It should be noted that some older studies denote $CRM(\%)$ and "$R$".

# 5 pTRM check statistics

## 5.1 pTRM checks

A pTRM check is a repeat TRM acquisition step to test for changes in a specimen's ability to acquire TRM at blocking temperatures below the temperature of the check. The difference between a pTRM check and the original TRM is calculated as the scalar intensity difference. That is,

$$\delta pTRM_{i,j} = pTRM\_check_{i,j} - TRM_i = pTRM\_check_{i,j} - x_i,$$

where $pTRM\_check_{i,j}$ is the pTRM check to the $i^{th}$ temperature step after heating to the $j^{th}$ temperature step. The order of the difference is such that pTRM checks smaller than the original TRM yield negative $\delta pTRM_{i,j}$ and pTRM checks larger than the original TRM give positive $\delta pTRM_{i,j}$. For a pTRM check to be included in the analysis, both $T_i$ and $T_j$ must be less than or equal to $T_{max}$.

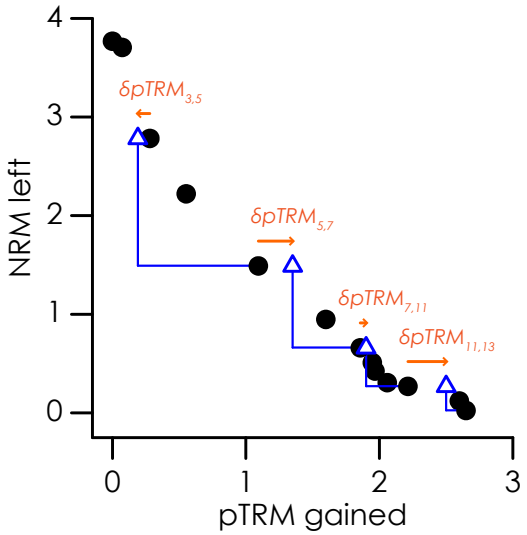


Figure 5: Schematic illustration of pTRM checks on an Arai plot and the quantities used to calculate pTRM check statistics.

**Statistic:** $n_{pTRM}$
The number of pTRM checks used to analyze the best-fit segment on the Arai plot (i.e., the number of $pTRM_{i,j}$ with $T_i \leq T_{max}$ and $T_j \leq T_{max}$).

## 5.2 Maximum pTRM check parameters

**Statistic:** $check(\%)$
*Report to 1 d.p.*

Maximum absolute difference produced by a pTRM check, normalized by the TRM acquired at that heating step.

$$check(\%) = \max\left\{\frac{|\delta pTRM_{i,j}|}{x_i} \times 100\right\}_{i \leq end \text{ and } j \leq end}$$

**Statistic:** $\delta CK$
*Report to 1 d.p.*

Maximum absolute difference produced by a pTRM check, normalized by the total TRM (obtained from the intersection of the best-fit line and the x-axis on an Arai plot; *Leonhardt et al.*, 2004a).

$$\delta CK = \frac{\max\left\{|\delta pTRM_{i,j}|\right\}_{i \leq end \textbf{ and } j \leq end}}{|X_{Int.}|} \times 100$$

**Statistic:** $DRAT$
*Report to 1 d.p.*

Maximum absolute difference produced by a pTRM check, normalized by the length of the best-fit line (*Selkin and Tauxe*, 2000).

$$DRAT = \frac{\max\left\{|\delta pTRM_{i,j}|\right\}_{i \leq end \textbf{ and } j \leq end}}{L} \times 100,$$

where $L$ is the length of the best-fit line on the Arai plot. $L$ is given by:

$$L = \sqrt{(\Delta x')^2 + (\Delta y')^2},$$

where $\Delta x'$ and $\Delta y'$ are TRM and NRM lengths of the best-fit line on the Arai plot, respectively (Section 3).

**Statistic:** $maxDEV$
*Report to 1 d.p.*

Maximum absolute difference produced by a pTRM check, normalized by the length of the TRM segment of the best-fit line on the Arai plot (*Blanco et al.*, 2012).

$$maxDEV = \frac{\max\left\{|\delta pTRM_{i,j}|\right\}_{i \leq end \textbf{ and } j \leq end}}{\Delta x'} \times 100$$

### 5.3 Cumulative pTRM check parameters

Most cumulative pTRM checks can be calculated in two fashions. The first method, is the summation of the signed pTRM differences (i.e., $\pm\delta pTRM$), the second is to calculate the sum of the absolute pTRM difference (i.e., $|\delta pTRM|$). The convention of the Standard Paleointensity Definition is to denote the second approach with a prime ($'$). For example, $CDRAT$ is calculated by the first method and $CDRAT'$ by the second.

**Statistic:** $CDRAT$
*Report to 1 d.p.*

Cumulative $DRAT$ (*Kissel and Laj*, 2004).

$$CDRAT = \frac{\left|\sum_{i=1}^{end} \delta pTRM_{i,j}\right|}{L} \times 100$$

$$CDRAT' = \frac{\sum_{i=1}^{end} |\delta pTRM_{i,j}|}{L} \times 100$$

**Statistic:** *DRATS*
*Report to 1 d.p.*

Cumulative pTRM check difference normalized by the pTRM gained at the maximum temperature used for the best-fit on the Arai diagram (*Tauxe and Staudigel*, 2004).

$$DRATS = \frac{\left|\sum_{i=1}^{end} \delta pTRM_{i,j}\right|}{x_{end}} \times 100$$

$$DRATS' = \frac{\sum_{i=1}^{end} |\delta pTRM_{i,j}|}{x_{end}} \times 100$$

**Statistic: Mean** *DRAT*
*Report to 1 d.p.*

The average difference produced by a pTRM check, normalized by the length of the best-fit line.

$$\text{Mean } DRAT = \frac{1}{n_{pTRM}} \frac{\left|\sum_{i=1}^{end} \delta pTRM_{i,j}\right|}{L} \times 100$$

$$\text{Mean } DRAT' = \frac{1}{n_{pTRM}} \frac{\sum_{i=1}^{end} |\delta pTRM_{i,j}|}{L} \times 100$$

**Statistic: Mean** *DEV*
*Report to 1 d.p.*

Mean deviation of a pTRM check (*Blanco et al.*, 2012).

$$\text{Mean } DEV = \frac{1}{n_{pTRM}} \frac{\left|\sum_{i=1}^{end} \delta pTRM_{i,j}\right|}{\Delta x'} \times 100$$

$$\text{Mean } DEV' = \frac{1}{n_{pTRM}} \frac{\sum_{i=1}^{end} |\delta pTRM_{i,j}|}{\Delta x'} \times 100.$$

**Statistic:** *δpal*
*Report to 1 d.p.*

A measure of cumulative alteration determined by the difference of the alteration corrected intensity estimate (*Valet et al.*, 1996) and the uncorrected estimate, normalized by the uncorrected estimate (*Leonhardt et al.*, 2004a).

We first calculate the cumulative sum of the pTRM checks up to the $i^{th}$ step of the experiment:

$$\mathbf{C}_i = \sum_{l=1}^{l=i} \delta \mathbf{pTRM}_{l,j}, \quad \text{for } i = 1, \ldots, n_{max},$$

where $\delta\mathbf{pTRM}_{l,j}$ is the ***vector*** difference between $\mathbf{TRM}_l$ and $\mathbf{pTRM\_check}_{l,j}$, i.e.,

$$\delta\mathbf{pTRM}_{l,j} = \mathbf{TRM}_l - \mathbf{pTRM\_check}_{l,j}.$$

When no pTRM check is performed $\delta\mathbf{pTRM}_l = [0, 0, 0]$.
The $\mathbf{TRM}_i$ vector is then corrected by adding the cumulative effect of the alteration, $\mathbf{C}_i$:

$$\mathbf{TRM}_i^* = \mathbf{TRM}_i + \mathbf{C}_i, \quad \text{for } i = 1, \ldots, n_{max}.$$

Since no pTRM check is performed at the first step:

$$\mathbf{TRM}_1^* = \mathbf{TRM}_1.$$

The corrected TRM values on the Arai plot ($x_i^*$) can be calculated by determining the vector lengths of $\mathbf{TRM}_i^*$. The corrected slope on the Arai plot ($b^*$) can be calculated using the selected points and the standard approach outlined in Section 3. $\delta pal$ is then given by:

$$\delta pal = \left| \frac{b - b^*}{b} \right| \times 100.$$

# 6 pTRM tails check statistics

## 6.1 pTRM tail checks

A pTRM tail check is a repeat demagnetization step to test for changes in a specimen's magnetization carried in the blocking temperature range above the temperature of the check. The difference between the first NRM measurement and the pTRM tail check is calculated as the scalar intensity difference:

$$\delta tail_i = tail\_check_i - NRM_i = tail\_check_i - y_i,$$

where $tail\_check_i$ is the pTRM tail check to the $i^{th}$ temperature step. The order of the difference is such that tail checks smaller than the original NRM yield negative $\delta tail_i$ and tail checks larger than the original NRM give positive $\delta tail_i$. For a pTRM tail check to be included in the analysis, $T_i$ must be less than or equal to $T_{max}$.

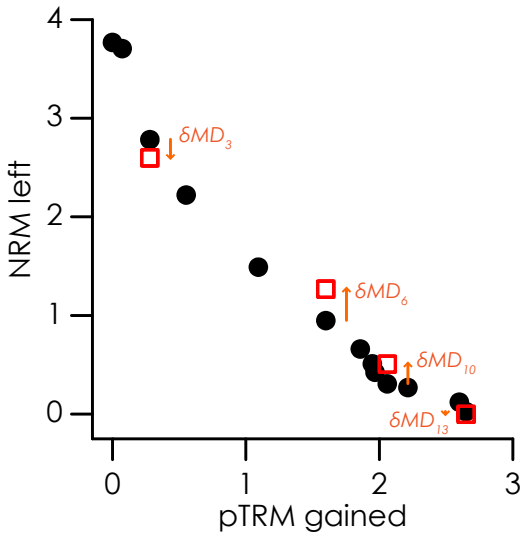


Figure 6: Schematic illustration of pTRM tail checks on an Arai plot and the quantities used to calculate pTRM tail check statistics.

**Statistic:** $n_{Tail}$
The number of pTRM tail checks conducted below the maximum temperature used for the best-fit segment on the Arai plot (i.e., the number of pTRM tail checks used to analyze the best-fit segment on the Arai plot).

**Statistic:** $DRAT_{Tail}$
*Report to 1 d.p.*

Maximum absolute difference produced by a pTRM tail check, normalized by the length of the best-fit line (*Biggin et al.*, 2007).

$$DRAT_{Tail} = \frac{\max\left\{|\delta tail_i|\right\}_{i=1,\ldots,end}}{L} \times 100$$

**Statistic:** $\delta TR$
*Report to 1 d.p.*

Maximum absolute difference produced by a pTRM tail check, normalized by the NRM (obtained from the intersection of the best-fit line and the y-axis on an Arai plot; *Leonhardt et al.*, 2004a).

$$\delta TR = \frac{\max\{|\delta tail_i|\}_{i=1,\ldots,end}}{|Y_{Int.}|} \times 100$$

**Statistic:** $MD_{VDS}$
*Report to 1 d.p.*

Maximum absolute difference produced by a pTRM tail check, normalized by the vector difference sum of the NRM (*Tauxe and Staudigel*, 2004).

$$MD_{VDS} = \frac{\max\{|\delta tail_i|\}_{i=1,\ldots,end}}{VDS} \times 100$$

**Statistic:** $\delta t^*$
*Report to 1 d.p.*

The extent of a pTRM tail after correction for angular dependence (*Leonhardt et al.*, 2004a,b).

The applied laboratory field vector ($\mathbf{B}_{Lab}$) is typically applied along a principle axis in the sample coordinate system (i.e., $\pm x$, $\pm y$, or $\pm z$). Therefore, for simplicity, $\delta t^*$ should be calculated in the sample coordinate system only. Figure 7 is a schematic illustration of aspects of the calculation of $\delta t^*$.

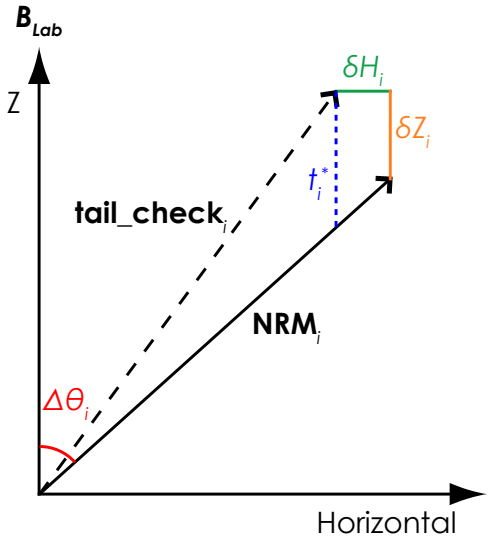


Figure 7: Schematic illustration of an NRM vector ($\mathbf{NRM}_i$) and a pTRM tail check vector ($\mathbf{tail\_check}_i$) for a sample that exhibits a pTRM tail. Modified after *Leonhardt et al.* (2004b).

Let $N_{x,i}$, $N_{y,i}$, and $N_{z,i}$ denote the Cartesian coordinates of the NRM vector at step $i$ (i.e., $\mathbf{NRM}_i = [N_{x,i}, N_{y,i}, N_{z,i}]$). Similarly, let $T_{x,i}$, $T_{y,i}$, and $T_{z,i}$ denote the Cartesian coordinates of the repeat demagnetization vector at step $i$ (i.e., $\mathbf{tail\_check}_i = [T_{x,i}, T_{y,i}, T_{z,i}]$).

Assuming that $\mathbf{B}_{Lab}$ is applied along the z-axis, the difference in the horizontal ($\delta H_i$) and vertical components ($\delta Z_i$) between $\mathbf{NRM}_i$ and $\mathbf{tail\_check}_i$ (Figure 7) are given by:

$$\delta H_i = \sqrt{N_{x,i}^2 + N_{y,i}^2} - \sqrt{T_{x,i}^2 + T_{y,i}^2}$$

and

$$\delta Z_i = N_{z,i} - T_{z,i}.$$

pTRM tails have an angular dependence and the calculation of $\delta t^*$ requires two angular differences. Let $\Delta\theta_i$ denote the angle between $\mathbf{B}_{Lab}$ and $\mathbf{NRM}_i$ (see Section 4 for advice on calculating the angle between two vectors). Let $\delta Inc_i$ denote the difference in inclinations between the $\mathbf{B}_{Lab}$ and $\mathbf{NRM}_i$:

$$\delta Inc_i = Inc(\mathbf{B}_{Lab}) - Inc(\mathbf{NRM}_i) = \arctan\left(\frac{B_{Lab,z}}{\sqrt{B_{Lab,x}^2 + B_{Lab,y}^2}}\right) - \arctan\left(\frac{N_{z,i}}{\sqrt{N_{x,i}^2 + N_{x,i}^2}}\right).$$

In the ThellierTool software (v4.22 and previous) $\mathbf{B}_{Lab}$ is determined from each $\mathbf{TRM}_i$. Given that $\mathbf{B}_{Lab}$ is almost always known, the convention of SPD is to use the known $\mathbf{B}_{Lab}$ and not as estimated from $\mathbf{TRM}_i$, which may suffer from the effects of experimental noise.

As will be seen below, the calculation of $\delta t^*$ requires $\frac{1}{\tan(\Delta\theta_i)}$. As $\Delta\theta_i$ approaches zero or 180° this fraction tends to infinity. To tackle this, $\delta t^*$ is calculated in a piecewise fashion that depends on upper and lower angular limits ($Lim_{upper}$ and $Lim_{lower}$, respectively). Below is pseudo-code that describes the logic of the calculation procedure.

**if** $\Delta\theta_i < Lim_{upper}$ **and** $\Delta\theta_i > Lim_{lower}$
**then**
  **if** $\delta Inc_i > 0$ **then**
    $t_i^* = 100 \times |b| \frac{-\delta Z_i + \frac{\delta H_i}{\tan(\Delta\theta_i)}}{|Y_{Int.}|}$
  **else**
    $t_i^* = 100 \times |b| \frac{\delta Z_i - \frac{\delta H_i}{\tan(\Delta\theta_i)}}{|Y_{Int.}|}$
  **end if**
**else**
  **if** $\Delta\theta_i \leq Lim_{lower}$ **then**
    $t_i^* = 0$
  **else if** $\Delta\theta_i \geq Lim_{upper}$ **then**
    $t_i^* = 100 \times \frac{-\delta Z_i}{|X_{Int.}| + |Y_{Int.}|}$
  **end if**
**end if**

In v4.22 of the ThellierTool $Lim_{lower} = 0.175$ ($\approx 10°$) radians and $Lim_{upper} = 2.968$ radians($\approx 170°$). These are adopted here.

$\delta t^*$ is then calculated as:

$$\delta t^* = \begin{cases} \max\{t_i^*\}_{i=1,\ldots,end} & \text{if } (\max\{t_i^*\}_{i=1,\ldots,end} > 0) \\ 0 & \text{if } (\max\{t_i^*\}_{i=1,\ldots,end} < 0) \end{cases}$$

Only positive values of $t^*$ and $\delta t^*$ can be attributed to the effects of pTRM tails, hence $\delta t^*$ is calculated as the maximum of $t^*$ and not the maximum of $|t^*|$.

It should be noted that an implicit assumption in the above calculations is that $\mathbf{B}_{Lab}$ is applied along the $z$-axis. In situations where $\mathbf{B}_{Lab}$ is applied along the $x$- or $y$-axes, the definition of "horizontal" and "vertical" can be redefined such that $\mathbf{B}_{Lab}$ is applied in the "vertical" direction. For example, if $\mathbf{B}_{Lab}$ is along the $x$-axis, $\delta H_i$ and $\delta Z_i$ can be defined as:

$$\delta H_i = \sqrt{N_{y,i}^2 + N_{z,i}^2} - \sqrt{T_{y,i}^2 + T_{z,i}^2}$$

and

$$\delta Z_i = N_{x,i} - T_{x,i},$$

and

$$\delta Inc_i = \arctan\left(\frac{B_{Lab,x}}{\sqrt{B_{Lab,y}^2 + B_{Lab,z}^2}}\right) - \arctan\left(\frac{N_{x,i}}{\sqrt{N_{y,i}^2 + N_{z,i}^2}}\right).$$

The remaining calculations can proceed as described above.

# 7 Additivity check statistics

## 7.1 Additivity checks

An additivity check is a repeat demagnetization step to test the validity of Thellier's law of additivity (*Krása et al.*, 2003). In the course of a paleointensity experiment, a pTRM at temperature $T_j$ is imparted, pTRM($T_j$, $T_0$), where $T_0$ is room temperature. An additivity check demagnetizes pTRM($T_j$, $T_0$) by heating to $T_i$, where $T_i < T_j$. The remaining pTRM (pTRM($T_j$, $T_i$)) is subtracted from the previous pTRM acquisition step, pTRM($T_j$, $T_0$), to estimate pTRM*($T_i$, $T_0$). That is

$$pTRM^*(T_i, T_0) = pTRM(T_j, T_0) - pTRM(T_j, T_i)$$

where * denotes an estimated value. This estimated value can be compared with a previously observed value of pTRM($T_i$, $T_0$) that was measured earlier in the experiment. The difference between the estimated and observed pTRMs is a measure of the violation of additivity between $T_i$ and $T_0$. The additivity check difference ($AC_{i,j}$) is the scalar intensity difference between the two pTRMs:

$$AC_{i,j} = pTRM^*(T_i, T_0) - pTRM(T_i, T_0).$$

For an additivity check to be included in the analysis, both $T_i$ and $T_j$ must be less than or equal to $T_{max}$.

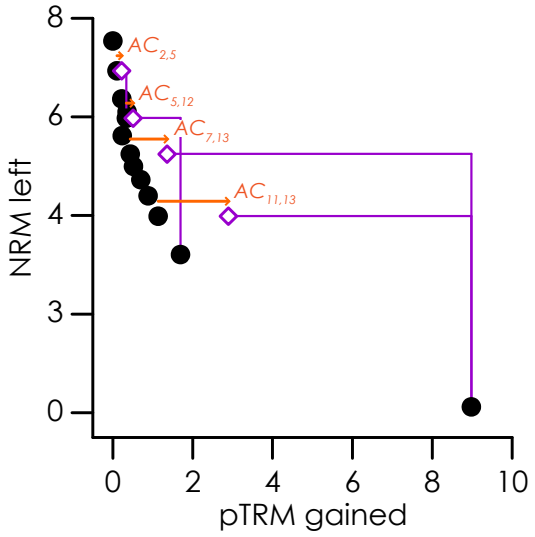


Figure 8: Schematic illustration of additivity checks on an Arai plot and the quantities used to calculate additivity check statistics.

**Statistic:** $n_{Add}$
The number of additivity checks used to analyze the best-fit segment on the Arai plot (i.e., the number of $AC_{i,j}$ with $T_i \leq T_{max}$ and $T_j \leq T_{max}$).

**Statistic:** $\delta AC$
*Report to 1 d.p.*

The maximum absolute additivity check difference normalized by the total TRM (obtained from

the intersection of the best-fit line and the x-axis on an Arai plot; *Leonhardt et al.*, 2004a).

$$\delta AC = \frac{\max\left\{|AC_{i,j}|\right\}_{i \leq end \textbf{ and } j \leq end}}{|X_{Int.}|} \times 100.$$

# 8 Anisotropic TRM

## 8.1 The basic procedure

Correction of paleointensity results for anisotropic TRM is based on the premise that in a weak magnetic field a TRM vector (**TRM**) is related to the applied field vector (**B**) by:

$$\mathbf{TRM} = \chi_{TRM}\mathbf{B},$$

where $\chi_{TRM}$ is the TRM anisotropy tensor, which is assumed to be temperature invariant (*Veitch et al.*, 1984; *Selkin et al.*, 2000). The anisotropy tensor can be experimentally determined by giving a specimen a full TRM or ARM in 6 different directions ($\pm x$, $\pm y$, $\pm z$).

To correct a paleointensity estimate, a unit vector in the direction of the ancient field ($\hat{\mathbf{B}}_{\mathbf{Anc}}$; the hat denotes a unit vector) must be determined. Given a unit vector in the direction of the characteristic NRM direction ($\hat{\mathbf{M}}_{\mathbf{ChRM}}$), $\hat{\mathbf{B}}_{\mathbf{Anc}}$ can be calculated from:

$$\hat{\mathbf{B}}_{\mathbf{Anc}} = \frac{\chi_{TRM}^{-1}\hat{\mathbf{M}}_{\mathbf{ChRM}}}{\left|\chi_{TRM}^{-1}\hat{\mathbf{M}}_{\mathbf{ChRM}}\right|}.$$

$\hat{\mathbf{M}}_{\mathbf{ChRM}}$ is determined from the free-floating PCA fit to the NRM steps from the selected Arai plot segment.

The paleointensity correction factor, $c$, which is the ratio of a magnetization gained in the direction of $\hat{\mathbf{B}}_{\mathbf{Lab}}$ to a magnetization gained in the direction of $\hat{\mathbf{B}}_{\mathbf{Anc}}$ can then be calculated as:

$$c = \frac{\left|\chi_{TRM}\hat{\mathbf{B}}_{\mathbf{Lab}}\right|}{\left|\chi_{TRM}\hat{\mathbf{B}}_{\mathbf{Anc}}\right|}. \tag{1}$$

The anisotropy corrected paleointensity estimate is simply given by:

$$B_{Anc} = cB_{Lab}\left|b\right|.$$

***Useful Note***...
Two methods to correct for anisotropy have been outlined in the literature (*Veitch et al.*, 1984; *Selkin et al.*, 2000). The method outlined above is that derived from *Veitch et al.* (1984), but both methods yield identical paleointensity estimates. The method of *Selkin et al.* (2000), however, can have a detrimental effect of some selection statistics and the method outlined above should be the preferred approach (*Paterson*, 2013).

## 8.2 Calculation of $\chi_{TRM}$

The anisotropy tensor, $\chi_{TRM}$, can be mathematically represented by a 3×3 matrix, which has 6 independent elements.

$$\chi_{TRM} = \begin{pmatrix} s_1 & s_4 & s_6 \\ s_4 & s_2 & s_5 \\ s_6 & s_5 & s_3 \end{pmatrix}$$

For convenience, we can define a column matrix, $\mathbf{s}$, which contains the 6 independent elements, $s_j, j = 1 \ldots 6$.

The TRM acquired when a specimen is placed in series of positions with respect to the applied field, can be expresses as

$$\mathbf{TRM}_i = \mathbf{A}_{i,j}\mathbf{s}_j,$$

where $i$ denotes the $i^{th}$ measurement position and $\mathbf{A}$ is know as the design matrix and depends on the experimental design (i.e., the sequence of axes along which the field is applied).

The typical 6 positions of measurement of $\chi_{TRM}$ or $\chi_{ARM}$ ($\pm x$, $\pm y$, $\pm z$) can be represented by the matrix $\mathbf{P}$, which contains the unit vectors of the axes along which $B_{Lab}$ is applied.

$$\mathbf{P} = \begin{pmatrix} P_{1,1} & P_{1,2} & P_{1,3} \\ P_{2,1} & P_{2,2} & P_{2,3} \\ \vdots & \vdots & \vdots \\ P_{6,1} & P_{6,2} & P_{6,3} \end{pmatrix}$$

For each element $P_{i,j}$ of $\mathbf{P}$, $i$ denotes the $i^{th}$ measurement position and $j = 1 \ldots 3$, denotes the Cartesian coordinates of the unit vector along which the remanence is acquired (i.e., $j = 1 = x$, $j = 2 = y$, $j = 3 = z$). The design matrix of such a routine is given by:

$$\mathbf{A} = \begin{pmatrix} P_{1,1} & 0 & 0 & P_{1,2} & 0 & P_{1,3} \\ 0 & P_{1,2} & 0 & P_{1,1} & P_{1,3} & 0 \\ 0 & 0 & P_{1,3} & 0 & P_{1,2} & P_{1,1} \\ P_{2,1} & 0 & 0 & P_{2,2} & 0 & P_{2,3} \\ 0 & P_{2,2} & 0 & P_{2,1} & P_{2,3} & 0 \\ 0 & 0 & P_{2,3} & 0 & P_{3,3} & P_{3,1} \\ P_{3,1} & 0 & 0 & P_{3,2} & 0 & P_{3,3} \\ 0 & P_{3,2} & 0 & P_{3,1} & P_{3,3} & 0 \\ 0 & 0 & P_{3,3} & 0 & P_{3,2} & P_{3,1} \\ P_{4,1} & 0 & 0 & P_{4,2} & 0 & P_{4,3} \\ 0 & P_{4,2} & 0 & P_{4,1} & P_{4,3} & 0 \\ 0 & 0 & P_{4,3} & 0 & P_{4,2} & P_{4,1} \\ P_{5,1} & 0 & 0 & P_{5,2} & 0 & P_{5,3} \\ 0 & P_{5,2} & 0 & P_{5,1} & P_{5,3} & 0 \\ 0 & 0 & P_{5,3} & 0 & P_{5,2} & P_{5,1} \\ P_{6,1} & 0 & 0 & P_{6,2} & 0 & P_{6,3} \\ 0 & P_{6,2} & 0 & P_{6,1} & P_{6,3} & 0 \\ 0 & 0 & P_{6,3} & 0 & P_{6,2} & P_{6,1} \end{pmatrix}.$$

***Numerical Tip...***
To allow flexibility, the below pseudo-code can be used to easily generate **A**, when **P** is variable.

**for** $i = 1 \rightarrow 6$ **do**
index=(3×(i-1))+1
A(index,1)=P(i,1)
A(index,2)=P(i,2)
A(index,3)=P(i,3)

A(index+1,1)=P(i,1)
A(index+1,2)=P(i,2)
A(index+1,3)=P(i,3)

A(index+2,1)=P(i,1)
A(index+2,2)=P(i,2)
A(index+2,3)=P(i,3)
**end for**

The best-fit values for **s** for the measured data can be obtained through the linear relationship:

$$\mathbf{s} = \left(\mathbf{A}^T\mathbf{A}\right)^{-1}\mathbf{A}^T\mathbf{TRM},$$

where $^T$ and $^{-1}$ denote the matrix transpose and inverse, respectively. These best-fit value then be used to construct $\chi_{TRM}$ and hence determine $c$.

***Numerical Tip...***
Calculating the inverse of the anisotropy tensor or $\left(\mathbf{A}^T\mathbf{A}\right)$ is not strictly necessary and can be inefficient and inaccurate. An alternative approach can be used if it is recognized that ${\chi^{-1}}_{TRM}\hat{\mathbf{M}}_{ChRM}$ and $\left(\mathbf{A}^T\mathbf{A}\right)^{-1}\mathbf{A}^T$ are linear problems of the form:

$$\mathbf{x} = \mathbf{A}^{-1}\mathbf{b}.$$

Many programming languages support tools that allow the solving of such linear systems without having to calculate the matrix inverse. For example, the `MATLAB` command `x=A\b` or the `Python` command `x=linalg.solve(A,b)` are solutions that do not need to calculate the inverse of **A**. Such approaches are numerically efficient and more stable and should be used where available.

$\chi_{TRM}$ is expressed in core coordinates, but much like the analysis of paleomagnetic directions, there exists an alternate coordinate system that that allows $\chi_{TRM}$ to be expressed in terms of principal components. That is,

$$\chi_{TRM}\mathbf{V} = \tau\mathbf{V}$$

where **V** is a matrix that contains the three eigenvectors (principal axes) and $\tau$ is a diagonal matrix that contains the three eigenvalues. The eigenvalues of the anisotropy tensor can then be used to characterize the anisotropy behaviour of a specimen (e.g., degree of anisotropy etc.) See *Tauxe* (2010) for further details.

### 8.3 Test for alteration after measurement of $\chi_{TRM}$

**Statistic:** $\delta TRM_{Anis}$
*Report to 1 d.p.*

To test for alteration during the measurement of $\chi_{TRM}$ a repeat remagnetization step is performed to the first treatment position. $\delta TRM_{Anis}$ is the difference between the intensities of the TRM acquired during first heating in position 1 ($TRM_{P1}$) and the second heating in position 1 ($TRM'_{P1}$) normalized by $TRM_{P1}$.

$$\delta TRM_{Anis} = \frac{|TRM_{P1} - TRM'_{P1}|}{TRM_{P1}} \times 100$$

# 9 Non-linear TRM

## 9.1 Theory and correction

An implicit assumption in paleointensity experiments is that TRM acquisition is linearly proportional to the applied field. However, both single domain theory (*Néel*, 1949) and experimental data (*Selkin et al.*, 2007) provide evidence that some particles can acquire TRM in a non-linear fashion in applied fields that are typical of the geomagnetic field intensity (i.e., $\lesssim 100$ $\mu$T).

Single domain theory (*Néel*, 1949) predicts that TRM is proportional the hyperbolic tangent of the applied field ($B$) as described by:

$$TRM = M_{rs} \tanh\left(\frac{V M_s(T_b) B}{k T_b}\right),$$

where $M_{rs}$ is the saturation remanent magnetization, $V$ is the grain volume, $M_s(T_b)$ is the saturation magnetization at the blocking temperature ($T_b$), and $k$ is the Boltzmann constant. For weak fields the linear approximation generally holds true for most SD grains and is a result of the approximation that $\tanh(x) \approx x$ for small $x$.

In comparison to Néel theory, *Selkin et al.* (2007) proposed that non-linear TRM acquisition be approximated by:

$$TRM = A_1 \tanh\left(A_2 B\right),$$

where $A_1$ and $A_2$ are scaling coefficients. It can be noted that the linear approximation is valid in the limit as $A_2$ tends to zero and that linearity of magnetization with applied field is a special case of the more general non-linear form. This simple approximation assumes that $A_2$ is temperature invariant, which in the strictest sense is not true $\left(A_2 \propto \frac{M_s(T_b)}{T_b}\right)$. This approximation, however, has been demonstrated to fit real data well (*Selkin et al.*, 2007; *Shaar et al.*, 2010) and the assumption of a temperature invariant $A_2$ is equivalent to assuming that the degree of non-linearity is identical for all pTRMs and total TRMs.

The non-linear behaviour of a specimen can be determined by imparting the specimen with TRMs acquired in a range of applied field. A best-fit hyperbolic tangent model (of the form given above) can then be fitted to the data to determine the $A_1$ and $A_2$ coefficients. For an SD specimen in the absence of chemical alteration (i.e., the coefficients $A_1$ and $A_2$ do not change), the slope of the line ($|b|$) on an Arai plot can be described by:

$$|b| = \frac{NRM_{Anc}}{TRM_{Lab}} = \frac{\tanh\left(A_2 B_{Anc}\right)}{\tanh\left(A_2 B_{Lab}\right)},$$

and $B_{Anc}$ is:

$$B_{Anc} = \frac{\tanh^{-1}\left(|b| \tanh\left(A_2 B_{Lab}\right)\right)}{A_2}.$$

## 9.2 Combined anisotropic and non-linear TRM correction

Many natural specimens, particularly archeological materials, suffer from both anisotropic and non-linear TRM and therefore must be corrected for both. This can be achieved using:

$$B_{Anc} = \frac{\tanh^{-1}\left(c\,|b| \tanh\left(A_2 B_{Lab}\right)\right)}{A_2}.$$

### 9.3 Test for alteration after measurement of $A_1$ and $A_2$

**Statistic:** $\delta TRM_{NLT}$
*Report to 1 d.p.*

To test for alteration during the measurement TRM acquisition a repeat remagnetization step is performed in the first laboratory field, which is typically the same field as used for the paleointensity experiment (i.e., the final TRM acquisition in $B_{Lab}$). $\delta TRM_{NLT}$ is the difference between the TRM acquire in first heating in $B_{Lab}$ ($TRM_{B_{Lab}}$) and the second heating in $B_{Lab}$ ($TRM'_{B_{Lab}}$) normalized by $TRM_{B_{Lab}}$.

$$\delta TRM_{NLT} = \frac{\left| TRM_{B_{Lab}} - TRM'_{B_{Lab}} \right|}{TRM_{B_{Lab}}} \times 100$$

# 10 The statistics of multiple paleointensity estimates

## 10.1 Averaging and weighting

**Statistic:** $N$
The number of paleointensity estimates to be analyzed.

**Statistic:** $B_j$
The value of the $j^{th}$ paleointensity estimate, where $j = 1$ to $N$.

**Statistic:** $m$
*Report to 1 d.p.*

The arithmetic mean of the $N$ paleointensity estimates

$$m = \frac{\sum_{j=1}^{N} B_j}{N}.$$

**Statistic:** $s$
*Report to 1 d.p.*

The standard deviation of the $N$ paleointensity estimates.

$$s = \left( \frac{\sum_{j=1}^{N} (B_j - m)^2}{N-1} \right)^{\frac{1}{2}}$$

**Statistic:** $m_w$
*Report to 1 d.p.*

The weighted mean of the $N$ paleointensity estimates.

$$m_w = \frac{\sum_{j=1}^{N} W_j B_j}{\sum_{j=1}^{N} W_j},$$

where $W_j$ is the weight on the $j^{th}$ paleointensity estimate.

**Statistic:** $s_w$
*Report to 1 d.p.*

The weighted standard deviation of the $N$ paleointensity estimates (*Heckert and Filliben*, 2003).

$$s_w = \left( \frac{N \sum_{j=1}^{N} W_j \left(B_j - m_w\right)^2}{(N-1) \sum_{j=1}^{N} W_j} \right)^{\frac{1}{2}}$$

***Useful Note...***
Several options are available to act as weights. Two options that have been used in the literature are the quality and weighting factors, $q$ and $w$, respectively. Their use as weighting factors, however, are not appropriate. As is outlined in Section 3, $w \propto q$, which itself is a function of the Arai plot slope ($|b|$). Hence, both $q$ and $w$ are proportional to the paleointensity estimate. If $q$ or $w$ are used as a weight ($W_j$) then $W_j \propto B_j$ (i.e., higher paleointensity estimates will tend to have larger weights), which can bias the weighted mean to higher values. Such dependencies should be carefully considered when deciding on the choice of which statistic to use for weighting.

## 10.2 Measures of scatter

**Statistic:** $\delta B(\%)$
*Report to 1 d.p.*

The standard deviation as a percentage of the mean value. Often referred to as the scatter.

$$\delta B(\%) = \frac{s}{m} \times 100$$

**Statistic:** $\delta B_N(\%)$
*Report to 1 d.p.*

When dealing with small numbers of data (i.e., small $N$), both $m$ and $s$ are inherently uncertain and these uncertainties propagate into measures of scatter. To account for this, *Paterson et al.* (2010a) proposed an adjustment to $\delta B(\%)$ to determine the upper 95% confidence interval ($\delta B_N(\%)$). Using this approach we can say, with 95% confidence, that the true scatter of the data is less than $\delta B_N(\%)$. This allows for a fairer comparison of data sets with different $N$.

$$\delta B_N(\%) = \left| \frac{\sqrt{N}}{t_{nc}\left(1-\alpha;\ (N-1);\ \frac{m\sqrt{N}}{s}\right)} \right| \times 100,$$

where $t_{nc}$ is the noncentral $t$ critical value for the $(1-\alpha)$ confidence level for $(N-1)$ degrees of freedom and with noncentrality parameter $\frac{m\sqrt{N}}{s}$.

## 10.3 Statistical tests for scatter

**Statistic:** $p_{\delta B}$
*Report to 3 d.p.*

An alternative approach is to determine the probability that the scatter (i.e., $\delta B(\%)$) is less than some critical value, $\delta B_{max}$ (*Paterson et al.*, 2010a). By adopting this approach, selection based on scatter can be performed as a statistical test, whereby we test the null hypothesis that our measured scatter is less than or equal to $\delta B_{max}$. The probability $p_{\delta_B}$ that this is the case is given by

$$p_{\delta B} = F_{nct}\left(\frac{\sqrt{N}}{\delta B_{max}};\ (N-1)\ ;\ \frac{m\sqrt{N}}{s}\right),$$

where $F_{nct}()$ is the noncentral $t$ cumulative distribution function and $\delta B_{max}$ is given as a fraction and not a percentage (e.g., 0.25 as opposed to 25%). If $p_{\delta_B} \leq 0.05$ we cannot reject the null hypothesis that our measured scatter is less than or equal to $\delta B_{max}$ (at the 5% significance level). If, however, $p_{\delta_B} > 0.05$ we can reject the null hypotheses and our measured scatter is most likely greater than $\delta B_{max}$. The two outlined approaches are identical, with $\delta B_N(\%)$ being the value of $\delta B_{max}$ that yields $p_{\delta_B} = 0.05$.

**Statistic:** $p_s$
*Report to 3 d.p.*

Some studies prefer to select data using an absolute limit on the standard deviation ($s_{max}$) of an average paleointensity estimate, most notably when the estimate is low and the relative scatter may therefore be high. Given that, under the assumption of normality, estimated variance follows a scaled chi-squared distribution the probability that $s$ is less than or equal to $s_{max}$ is given by

$$p_s = F_{\chi^2}\left(\frac{(N-1)s_{max}^2}{s^2};\ (N-1)\right),$$

where $F_{\chi^2}()$ chi-squared cumulative distribution function with $N-1$ degrees of freedom. If $p_s \leq 0.05$ we cannot reject the null hypothesis that our measured scatter is less than or equal to $s_{max}$ (at the 5% significance level). If, however, $p_s > 0.05$ we can reject the null hypotheses and our measured scatter is most likely greater than $s_{max}$.

It should be noted that, in case where $\delta B_{max} = \frac{s_{max}}{m}$, $p_s$ is always less than $p_{\delta B}$. This is due to fact that $p_{\delta B}$ accounts for sample size related uncertainty in both $m$ and $s$, but $p_s$ accounts for sample size uncertainty in only $s$.

# 11 Calibration data set

To be able to test and calibrate the calculation of paleointensity data across multiple platforms and software bases, we have provided a data set of 20 paleointensity specimens with which users can test their software. The data set can be downloaded from http://www.paleomag.net/SPD/downloads.html in either MagIC or ThellierTool format.

## 11.1 Data sources

The 20 specimens used for testing and calibration are drawn from the compilation of data from historical location compiled by *Paterson et al.* (2013). The data are from 12 studies and represent 15 localities or laboratory experiments (16 unique heating events). The methods and materials used are outlined in Table 1. The data from *Selkin et al.* (2000) and *Shaar et al.* (2010) are corrected for the effects of non-linear TRM and/or anisotropy. The non-linear TRM coefficients (i.e., $A_1$ and $A_2$) as well as the six unique elements required to construct the anisotropy tensors (i.e., $s_{j=1...6}$) are available as text files to download from http://www.paleomag.net/SPD/downloads.html.

## 11.2 Standardized parameters

A complete table of the standard paleointensity statistics and the details of the chosen best-fits for the above 20 specimens is available for download from http://www.paleomag.net/SPD/downloads.html. For the calculation of statistics that make a comparison with a known reference direction (e.g., $\alpha'$, or $CRM(\%)$) an arbitrary reference direction is used. This direction is Dec. $= 90°$, Inc $= 45°$, or $\left[0, \frac{1}{\sqrt{2}}, \frac{1}{\sqrt{2}}\right]$ in Cartesian coordinates. For the calculation of $SCAT$, $\beta_{threshold}$ is taken to be 0.1.

Table 1: Meta-data of the 20 specimens provide to test and calibrate with SPD.

| Sample name | Reference | Location | pTRM checks | pTRM tail checks | Additivity checks | Method | Material | Comment |
|---|---|---|---|---|---|---|---|---|
| 187A | *Biggin et al.* (2007) | Mt. Etna, 1979 | Yes | Yes | No | MW Coe | Basaltic lava | With AF cleaning |
| 283A | *Biggin et al.* (2007) | Mt. Etna, 1950 | Yes | Yes | No | MW Coe | Basaltic lava | |
| A-3-3 | *Yamamoto et al.* (2003) | Hawaii, 1960 | Yes | No | No | Coe | Basaltic lava | |
| AL2770-3b | *Bowles et al.* (2006) | East Pacific Rise, 1991/92 | Yes | No | No | Coe | SBG | |
| BR06-4F | *Donadini et al.* (2007) | Helsinki, 1906 | Yes | Yes | No | Coe | Brick | |
| C-4-4L | *Yamamoto et al.* (2003) | Hawaii, 1960 | Yes | No | No | Coe | Basaltic lava | With low temperature demagnetization |
| HEL2-2d | *Donadini et al.* (2007) | Helsinki, 1906 | Yes | Yes | No | Coe | Brick | |
| KF-3-1 | *Tanaka et al.* (2012) | Krafla, 1984 | Yes | No | No | Coe | Basaltic lava | |
| LV6C3A | *Paterson et al.* (2010b) | Láscar, 1993 | Yes | Yes | No | Coe | Andesitic clast | |
| m428b1 | *Selkin et al.* (2000) | Stillwater Complex | Yes | No | No | Coe | Anorthosite | Anisotropic TRM corrected |
| MCT | *Muxworthy* (1998) | N/A | No | Yes | No | Coe | Synthetic magnetite | Average grain size 22.5 $\mu$m |
| MSH6E13 | *Paterson et al.* (2010b) | Mt. St. Helens, 1980 | Yes | Yes | Yes | Coe | Dacitic clast | |
| P1MY | *Muxworthy et al.* (2011) | Parícutin, 1943 | Yes | Yes | No | Coe | Basaltic lava | |
| RD2358-4f | *Pick and Tauxe* (1993) | East Pacific Rise, 1990 | Yes | Yes | No | Coe | SBG | |
| RS25b | *Shaar et al.* (2010) | N/A | Yes | No | No | IZZI | Remelted copper slag | Anisotropic and non-linear TRM corrected |
| RS26a | *Shaar et al.* (2010) | N/A | Yes | No | No | IZZI | Remelted copper slag | Anisotropic and non-linear TRM corrected |
| RS26e | *Shaar et al.* (2010) | N/A | Yes | No | No | IZZI | Remelted copper slag | Anisotropic and non-linear TRM corrected |
| TS01-20A-2 | *Yamamoto and Hoshi* (2008) | Sakurajima, 1914 | Yes | Yes | No | Coe | Andesitic lava | |
| VM1F | *Muxworthy et al.* (2011) | Vesuvius, 1940 | Yes | Yes | No | Coe | Basaltic lava | |
| W3 | *Krása et al.* (2003) | N/A | Yes | Yes | Yes | Coe | Synthetic magnetite | Average grain size 0.5 $\mu$m |

### 11.3 Averaging and descriptive statistics

The paleointensity estimates along with the average, standard deviation and scatter for the 20 specimens are given in Table 2. This table is also available for download as an Excel spreadsheet from http://www.paleomag.net/SPD/downloads.html.

Table 2: Paleointensity estimates and average value with associated descriptive statistics.

| Sample name | $B_{Exp}$ ($\mu$T) | $B_{Anc}$ ($\mu$T) |
|---|---|---|
| 187A | 44.1 | 45.2 |
| 283A | 43.3 | 116.3 |
| A-3-3 | 36.2 | 35.6 |
| AL2770-3b | 35.8 | 26.0 |
| BR06-4F | 49.6 | 41.9 |
| C-4-4L | 36.2 | 36.1 |
| HEL2-2d | 49.6 | 49.5 |
| KF-3-1 | 52.1 | 44.1 |
| LV6C3A | 24.0 | 23.4 |
| m428b1 | 25.0 | 25.1 |
| MCT | 55.6 | 71.7 |
| MSH6E13 | 55.6 | 22.1 |
| P1MY | 45.0 | 30.1 |
| RD2358-4f | 37.0 | 85.7 |
| RS25b | 30.0 | 29.3 |
| RS26a | 60.0 | 63.3 |
| RS26e | 60.0 | 58.1 |
| TS01-20A-2 | 45.7 | 50.1 |
| VM1F | 44.0 | 74.0 |
| W3 | 60.0 | 60.7 |
| | | |
| | $N$ | 20 |
| | $m$ ($\mu$T) | 49.4 |
| | $s$ ($\mu$T) | 24.2 |
| | $\delta B$(%) | 48.9 |
| | $\delta B_N$(%) | 66.3 |

#### 11.3.1 Weighting

An example of the calculation of weighted average and standard deviation of the above described data set is given in the Excel spreadsheet available for download from http://www.paleomag.net/SPD/downloads.html. In this example, the weights are taken to be $\frac{1}{(\sigma_B)^2}$.

## References

Biggin, A. J., M. Perrin, and M. J. Dekkers (2007), A reliable absolute palaeointensity determination obtained from a non-ideal recorder, *Earth Planet. Sci. Lett.*, *257*, 545–563, doi:10.1016/j.epsl.2007.03.017.

Blanco, D., V. A. Kravchinsky, J.-P. Valet, A. Ali, and D. K. Potter (2012), Does the Permo-Triassic geomagnetic dipole low exist?, *Phys. Earth Planet. Inter.*, *204–205*, 11–21, doi:10.1016/j.pepi.2012.06.005.

Bowles, J., J. S. Gee, D. V. Kent, M. R. Perfit, S. A. Soule, and D. J. Fornari (2006), Paleointensity applications to timing and extent of eruptive activity, 9°–10°N East Pacific Rise, *Geochem. Geophys. Geosyst.*, *7*, Q06006, doi:10.1029/2005gc001141.

Chernov, N., and C. Lesort (2005), Least squares fitting of circles, *J. Math. Imaging Vis.*, *23*, 239–252, doi:10.1007/s10851-005-0482-8.

Coe, R. S., S. Grommé, and E. A. Mankinen (1978), Geomagnetic paleointensities from radiocarbon-dated lava flows on Hawaii and the question of the Pacific nondipole low, *J. Geophys. Res.*, *83*, 1740–1756, doi:10.1029/JB083iB04p01740.

Coe, R. S., S. Grommé, and E. A. Mankinen (1984), Geomagnetic paleointensities from excursion sequences in lavas on Oahu, Hawaii, *J. Geophys. Res.*, *89*, 1059–1069, doi:10.1029/JB089iB02p01059.

Donadini, F., M. Kovacheva, M. Kostadinova, L. Casas, and L. J. Pesonen (2007), New archaeointensity results from Scandinavia and Bulgaria: Rock-magnetic studies inference and geophysical application, *Phys. Earth Planet. Inter.*, *165*, 229–247, doi:10.1016/j.pepi.2007.10.002.

Heckert, N. A., and J. J. Filliben (2003), *NIST Handbook 148: Dataplot Reference Manual, Volume 2: Let Subcommands and Library Functions*, National Institute of Standards and Technology Handbook Series.

Kirschvink, J. L. (1980), The least-squares line and plane and the analysis of palaeomagnetic data, *Geophys. J. R. Astr. Soc.*, *62*, 699–718, doi:10.1111/j.1365-246X.1980.tb02601.x.

Kissel, C., and C. Laj (2004), Improvements in procedure and paleointensity selection criteria (PICRIT-03) for Thellier and Thellier determinations: Application to Hawaiian basaltic long cores, *Phys. Earth Planet. Inter.*, *147*, 155–169, doi:10.1016/j.pepi.2004.06.010.

Krása, D., C. Heunemann, R. Leonhardt, and N. Petersen (2003), Experimental procedure to detect multidomain remanence during Thellier-Thellier experiments, *Phys. Chem. Earth*, *28*, 681–687, doi:10.1016/S1474-7065(03)00122-0.

Leonhardt, R., C. Heunemann, and D. Krása (2004a), Analyzing absolute paleointensity determinations: Acceptance criteria and the software ThellierTool4.0, *Geochem. Geophys. Geosyst.*, *5*, Q12016, doi:10.1029/2004GC000807.

Leonhardt, R., D. Krása, and R. S. Coe (2004b), Multidomain behavior during Thellier paleointensity experiments: A phenomenological model, *Phys. Earth Planet. Inter.*, *147*, 127–140, doi:10.1016/j.pepi.2004.01.009.

Muxworthy, A. R. (1998), Stability of magnetic remanence in multidomain magnetite, Ph.D. thesis.

Muxworthy, A. R., D. Heslop, G. A. Paterson, and D. Michalk (2011), A Preisach method for estimating absolute paleofield intensity under the constraint of using only isothermal measurements: 2. Experimental testing, *J. Geophys. Res.*, *116*, B04103, doi:10.1029/2010jb007844.

Néel, L. (1949), Théorie du traînage magnétique des ferromagnétiques en grains fins avec applications aux terres cuites, *Ann. Géophys.*, *5*, 99–136.

Paterson, G. A. (2011), A simple test for the presence of multidomain behaviour during paleointensity experiments, *J. Geophys. Res.*, *116*, B10104, doi:10.1029/2011JB008369.

Paterson, G. A. (2013), The effects of anisotropic and non-linear thermoremanent magnetizations on Thellier-type paleointensity data, *Geophys. J. Int.*, *193*, 694–710, doi:10.1093/gji/ggt033.

Paterson, G. A., D. Heslop, and A. R. Muxworthy (2010a), Deriving confidence in paleointensity estimates, *Geochem. Geophys. Geosyst.*, *11*, Q07Z18, doi:10.1029/2010gc003071.

Paterson, G. A., A. R. Muxworthy, A. P. Roberts, and C. Mac Niocaill (2010b), Assessment of the usefulness of lithic clasts from pyroclastic deposits for paleointensity determination, *J. Geophys. Res.*, *115*, B03104, doi:10.1029/2009JB006475.

Paterson, G. A., L. Tauxe, A. J. Biggin, R. Shaar, and L. C. Jonestrask (2014), On improving the selection of Thellier-type paleointensity data, *Geochem. Geophys. Geosyst.*, doi:10.1002/2013GC005135.

Pick, T., and L. Tauxe (1993), Geomagnetic palaeointensities during the Cretaceous normal superchron measured using submarine basaltic glass, *Nature*, *366*, 238–242, doi:10.1038/366238a0.

Prévot, M., E. A. Mankinen, R. S. Coe, and C. S. Grommé (1985), The Steens Mountain (Oregon) geomagnetic polarity transition: 2. Field intensity variations and discussion of reversal models, *J. Geophys. Res.*, *90*, 10,417–10,448, doi:10.1029/JB090iB12p10417.

Selkin, P. A., and L. Tauxe (2000), Long-term variations in palaeointensity, *Phil. Trans. R. Soc. London*, *358*, 1065–1088, doi:10.1098/rsta.2000.0574.

Selkin, P. A., W. P. Meurer, A. J. Newell, J. S. Gee, and L. Tauxe (2000), The effect of remanence anisotropy on paleointensity estimates: A case study from the Archean Stillwater Complex, *Earth Planet. Sci. Lett.*, *183*, 403–416, doi:10.1016/S0012-821X(00)00292-2.

Selkin, P. A., J. S. Gee, and L. Tauxe (2007), Nonlinear thermoremanence acquisition and implications for paleointensity data, *Earth Planet. Sci. Lett.*, *256*, 81–89, doi:10.1016/j.epsl.2007.01.017.

Shaar, R., and L. Tauxe (2013), Thellier GUI: An integrated tool for analyzing paleointensity data from Thellier-type experiments, *Geochem. Geophys. Geosyst.*, *14*, 677–692, doi:10.1002/ggge.20062.

Shaar, R., H. Ron, L. Tauxe, R. Kessel, A. Agnon, E. Ben-Yosef, and J. M. Feinberg (2010), Testing the accuracy of absolute intensity estimates of the ancient geomagnetic field using copper slag material, *Earth Planet. Sci. Lett.*, *290*, 201–213, doi:10.1016/j.epsl.2009.12.022.

Shaar, R., H. Ron, L. Tauxe, R. Kessel, and A. Agnon (2011), Paleomagnetic field intensity derived from non-SD: Testing the Thellier IZZI technique on MD slag and a new bootstrap procedure, *Earth Planet. Sci. Lett.*, *310*, 213–224, doi:10.1016/j.epsl.2011.08.024.

Tanaka, H., and T. Kobayashi (2003), Paleomagnetism of the late Quaternary Ontake Volcano, Japan: directions, intensities, and excursions, *Earth Planets Space*, *55*, 189–202.

Tanaka, H., Y. Hashimoto, and N. Morita (2012), Palaeointensity determinations from historical and Holocene basalt lavas in Iceland, *Geophys. J. Int.*, *189*, 833–845, doi:10.1111/j.1365-246X.2012.05412.x.

Tauxe, L. (2010), *Essentials of Paleomagnetism*, University of California Press, Berkeley.

Tauxe, L., and H. Staudigel (2004), Strength of the geomagnetic field in the Cretaceous Normal Superchron: New data from submarine basaltic glass of the Troodos Ophiolite, *Geochem. Geophys. Geosyst.*, *5*, Q02H06, doi:10.1029/2003GC000635.

Valet, J.-P., X. Quidelleur, E. Tric, P. Y. Gillot, J. Brassart, I. Le Meur, and V. Soler (1996), Absolute paleointensity and magnetomineralogical changes, *J. Geophys. Res.*, *101*, 25,029–25,044.

Veitch, R. J., I. G. Hedley, and J.-J. Wagner (1984), An investigation of the intensity of the geomagnetic-field during roman times using magnetically anisotropic bricks and tiles, *Arch. Sci.*, *37*, 359–373.

Warton, D. I., I. J. Wright, D. S. Falster, and M. Westoby (2006), Bivariate line-fitting methods for allometry, *Biol. Rev.*, *81*, 259–291, doi:10.1017/s1464793106007007.

Yamamoto, Y., and H. Hoshi (2008), Paleomagnetic and rock magnetic studies of the Sakurajima 1914 and 1946 andesitic lavas from Japan: A comparison of the LTD-DHT Shaw and Thellier paleointensity methods, *Phys. Earth Planet. Inter.*, *167*, 118–143, doi:10.1016/j.pepi.2008.03.006.

Yamamoto, Y., H. Tsunakawa, and H. Shibuya (2003), Palaeointensity study of the Hawaiian 1960 lava: implications for possible causes of erroneously high intensities, *Geophys. J. Int.*, *153*, 263–276, doi:10.1046/j.1365-246X.2003.01909.x.

York, D. (1966), Least-squares fitting of a straight line, *Can. J. Phys.*, *44*, 1079–1086, doi:10.1139/p66-090.

Yu, Y. (2012), High-fidelity paleointensity determination from historic volcanoes in Japan, *J. Geophys. Res.*, *117*, B08101, doi:10.1029/2012jb009368.

Yu, Y. J., and L. Tauxe (2005), Testing the IZZI protocol of geomagnetic field intensity determination, *Geochem. Geophys. Geosyst.*, *6*, Q06H11, doi:10.1029/2004GC000840.

Yu, Y. J., L. Tauxe, and A. Genevey (2004), Toward an optimal geomagnetic field intensity determination technique, *Geochem. Geophys. Geosyst.*, *5*, Q02H07, doi:10.1029/2003GC000630.